139 (2022) 212966

Contents lists available at ScienceDirect

Biomaterials Advances

journal homepage: www.journals.elsevier.com/materials-science-and-engineering-c

Biodegradable particles for protein delivery: Estimation of the release kinetics inside cells

Mikhail V. Zyuzin [a,*], Raimo Hartmann [b], Alexander S. Timin [a,c], Susana Carregal-Romero [d,e,f], Wolfgang J. Parak [g], Alberto Escudero [h,i,*]

[a] Department of Physics and Engineering, ITMO University, Lomonosova 9, St. Petersburg 191002, Russia
[b] Fachbereich Physik, Philipps Universität Marburg, 35037 Marburg, Germany
[c] Peter The Great St. Petersburg Polytechnic University, Polytechnicheskaya 29, St. Petersburg 195251, Russian Federation
[d] Center for Cooperative Research in Biomaterials (CIC biomaGUNE), Basque Research and Technology Alliance (BRTA), 20014 San Sebastián, Spain
[e] CIBER Enfermedades Respiratorias (CIBERES) Madrid, Spain
[f] Ikerbasque, Basque Foundation for Science, Bilbao 48013, Spain
[g] CHyN, Universität Hamburg, Hamburg, Germany
[h] Departamento de Química Inorgánica, Facultad de Química, Universidad de Sevilla, Calle Profesor García González 1, E–41012 Seville, Spain
[i] Instituto de Investigaciones Químicas (IIQ), Universidad de Sevilla – CSIC, Calle Américo Vespucio 49, E–41092 Seville, Spain

ARTICLE INFO

Keywords:
Drug delivery
Drug release
Proteins
Carrier
Capsules
In vitro
Kinetics

ABSTRACT

A methodology to quantify the efficiency of the protein loading and in-vitro delivery for biodegradable capsules with different architectures based on polyelectrolytes (dextran sulfate, poly-L-arginine and polyethylenimine) and SiO_2 was developed. The capsules were loaded with model proteins such as ovalbumin and green fluorescent protein (GFP), and the protein release profile inside cells (either macrophages or HeLa cells) after endocytosis was analysed. Both, protein loading and release kinetics were evaluated by analysing confocal laser scanning microscopy images using MatLab and CellProfiler software. Our results indicate that silica capsules showed the most efficient release of proteins as cargo molecules within 48 h, as compared to their polymeric counterparts. This developed method for the analysis of the intracellular cargo release kinetics from carrier structures could be used in the future for a better control of drug release profiles.

1. Introduction

The design of appropriate materials is a key factor in the field of drug delivery [1]. Free drugs often suffer from poor solubility and stability, and may show unwanted toxicity and/or an inability to cross cell plasma membranes [2,3]. In general, drugs can advantageously be associated with nano- or microparticulate carriers, which may act not only as a protective material, but also can orient their delivery [4]. Particle-based carriers are in general endocytosed, which allows for transport of the attached drugs into cells. However, inside cells the particles are in general trapped inside intracellular vesicles such as endosomes and lysosomes [5,6]. Apart from the problematics of having to leave these vesicles in order to reach the cytosol (the so-called endosomal escape dilemma), the drugs also need to be released from their particle carrier at the site of action [7,8]. A proper drug release kinetics is required to achieve an efficient treatment efficiency and a safety profile. Depending on the size, shape, and surface properties, nano- and microparticles can systematically circulate in the blood for a prolonged periods, accumulate in tumoral regions, and locally release drugs [9,10]. Depending on the carrier nature, drug release can occur either in burst-like [11–13] or in prolonged manner [14,15], which can be used to maximize the efficiency of therapy. In some cases, drug release from nano- and microparticles should be slow enough in order to provide prolonged drug action at necessary therapeutic concentrations. For instance, treatments with antibiotics often require sustainable action over an increased period of time (2–3 weeks) in the local injury area [16,17]. Therefore, an appropriate drug release kinetics from nano- and microparticles is an essential factor in their design and one important feature concerning the therapeutic abilities and potential for clinical use.

There are a number of analytical techniques that allow to quantify the amount of loaded and released cargo molecules from nano- and microparticles. Particularly, High Performance Liquid Chromatography

* Corresponding authors.
E-mail addresses: mikhail.zyuzin@metalab.ifmo.ru (M.V. Zyuzin), alberto.escudero@csic.es (A. Escudero).

https://doi.org/10.1016/j.bioadv.2022.212966
Received 18 February 2022; Received in revised form 17 May 2022; Accepted 28 May 2022
Available online 1 June 2022

(HPLC) is capable to directly read the characteristic absorbance of loaded compounds upon elution from a proper HPLC column [18]. However, this method is limited by its inability of real-time monitoring of release from nano- and microparticles. Another approach to monitor drug release kinetics is to load nano- and microparticles into dialysis devices with a molecular weight cut-off larger than the size of the drug molecules. Drug carriers are then continuously dialyzed into biological fluids (e.g., phosphate-buffered saline, PBS) and the released drugs diffuse through the dialysis membranes due to osmotic pressure. Afterwards, small volumes of dialysis solutions are analysed using fluorescence measurements, UV–vis absorption spectroscopy, or other techniques to detect the released drug molecules [19]. As a drawback, the sensitivity of dialysis approaches is a critical issue. Apart from dialysis, released drug molecules can also be separated from the carrier particles by centrifugation [20]. All above-mentioned approaches to measure drug release kinetics from nano- and microcarriers act outside cells, i.e. in the test tube [21]. The intracellular environment can however be significantly different and more complex than biological fluids in the test tubes, which can modify the drug release profile from the carriers.

Therefore, a good understanding of the intracellular nanoparticle trafficking and kinetics is demanded for the efficient delivery of nanoparticles or carriers. Several approaches for the study of the kinetics of the interaction between drug nanocarriers and cells have been reported in the literature. This includes the monitoring of the intracellular release and distribution of nanostructures [22].

In some cases, cargos can be delivered without using a carrier. This is known as membrane disruption-mediated intracellular delivery [23] and, for example, the analysis of the fluorescence of a fluorescent cargo with increasing times can be used to study its intracellular release kinetics [24]. For the cases in which a carrier is required, strategies involving the quantification of the particle number or dose inside the cells with increasing times have been reported. For example, TEM has been used to monitor the kinetics of the intracellular distribution of surface-modified gold nanoparticles with time. This allows to distinguish between the cytoplasm and the organelles [25]. Additionally, and depending on the cargo nature, its release from the carrier can also be determined. This is the case of the intracellular RNA delivery from lipid nanoparticles, which has been analysed by optical tracking of siRNAs [26] or by considering the proteins produced via mRNA translation [27,28]. For some particles, the quantification of the nanoparticle dose with cell proliferation has also been determined [29].

Focusing on the delivery of cargo from appropriate carriers, alternative approaches to monitor in-vitro the release and the kinetics of the released loaded cargo molecules (i.e., drugs) are thus required. In this work, various biodegradable hollow microparticles (capsules) made of SiO_2 and different polymers were used as particulate carriers. Capsules have been frequently used for the in-vitro delivery of different drugs and biomolecules [15,30–32], such as proteins and gene material, and show also some applications in-vivo [33], including the therapy of cancer [34].

The capsules used in this study were loaded with fluorescent-labelled proteins as cargo molecules in order to allow for fluorescence-based estimation of their loading efficiency and their in-vitro protein release. For this, a methodology for the loading and release evaluation based on confocal laser scanning microscopy (CLSM) imaging and image processing using the open source Matlab and CellProfiler software was developed. The proposed analysis was also used to monitor the release kinetics from different polymer capsules inside cells.

2. Materials and methods

2.1. Synthesis of capsules

Different types of biodegradable capsules loaded either with DQ-ovalbumin (DQ-OVA) or with green fluorescent protein (GFP) were synthesized as reported elsewhere [35–37]. We used the following polyelectrolytes: dextran sulfate (DEXS), poly-L-arginine (PARG), polyethylenimine (PEI), poly(sodium 4-styrenesulfonate) (PSS), and poly allylamine (PAH). The following capsule architectures were prepared: (i) $(DEXS/PARG)_3$, (ii) $(DEXS/PARG)_4$, (iii) $(DEXS/PARG)_2/DEXS/PEI/DEXS/PARG$, (from here on, in order to facilitate the reading, we assigned these PEI-based capsules a shorter name: $(DEXS/PEI\text{-}or\text{-}PARG)_4$), and (iv) SiO_2/poly-L-arginine (SiO_2/PARG). As control, (v) non-biodegradable $(PSS/PAH)_4$ were used [30,38]. All the capsule types were characterized using scanning electron microscopy (SEM), scanning transmission electron microscopy (STEM), and confocal laser scanning microscopy (CLSM). The detailed protocols are described in the Supplementary Data.

2.2. Stability and loading of the capsules

The spontaneous release (i.e., leaching) of DQ-OVA from DQ-OVA loaded capsules was checked in full cell culture medium using CLSM imaging during 48 h. The amount of remaining encapsulated fluorescent DQ-OVA was estimated in terms of intensity of its fluorescence signal using CLSM image processing. The detailed protocols are described in the Supplementary Data.

2.3. Release studies outside and inside cells

To study the degradation-triggered DQ-OVA release, capsules of different types were incubated in pronase-containing solution for different time periods. The amount of the released DQ-OVA was analysed with a fluorimeter. In order to study the release profile of DQ-OVA or GFP inside cells, capsules of different types were incubated with RAW 264.7 or HeLa cells and imaged with CLSM for 48 h. The CLSM images were processed with the Matlab and CellProfiler software. The detailed protocols are described in the Supplementary Data.

3. Results and discussion

The strategy of this study is presented in Scheme 1. Capsules composed of different polymers (either synthetic or natural) and SiO_2 and loaded with different proteins (either DQ-OVA or GFP) were synthesized and characterized using confocal laser scanning microscopy

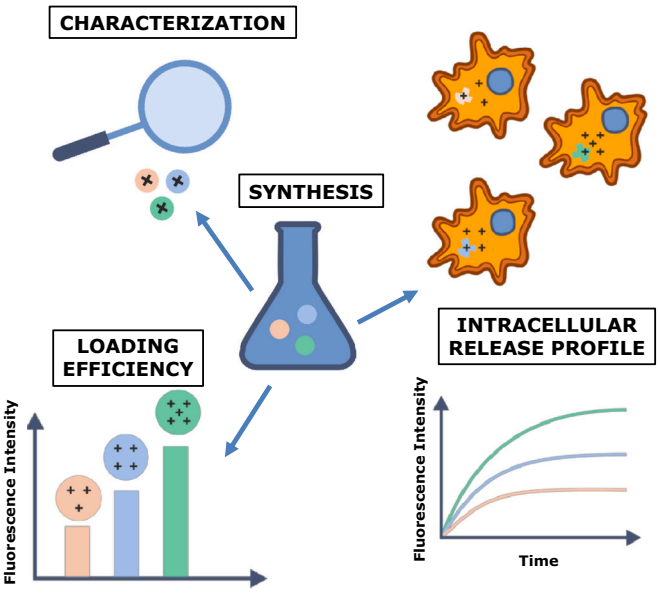

Scheme 1. Schematic illustration of implemented steps of synthesis, characterization, estimation of loading efficiency and release profiles of capsules inside and outside cells.

(CLSM). The loading efficiency of the different capsules, the stability of the obtained capsules in biological fluids, and the protein release outside and inside cells within 48 h were estimated using CLSM images processed with the Matlab and CellProfiler software.

3.1. Characterization and loading of capsules

The synthesis of the DQ-OVA loaded capsules with different architectures yielded micrometric sized capsules, as inferred from SEM/STEM images (Fig. 1). SEM images collected for dried polyelectrolyte-based capsule samples show collapsed structures. However, the different CLSM images taken for capsule suspensions in water (Fig. 2 and Figs. S1 and S2) indicate that they are spherical. STEM images of SiO_2/PARG capsules demonstrate the formation of hollow spheres. Given the inorganic nature of the capsule, they do not collapse when drying.

The fluorescence of the protein DQ-OVA was used to estimate the loading efficiency in the capsules with different architectures and to study the kinetics of the cargo release. DQ-OVA consists of the protein ovalbumin labelled with the green dye BODIPY (excitation/emission at $\lambda_{exc.}/\lambda_{em.} = 503/512$ nm). The dye molecules are almost completely self-quenched due to their close proximity and thus high density in the protein. Intact DQ-OVA (i.e., as originally loaded into the capsules) shows red fluorescence ($\lambda_{exc.}/\lambda_{em.} = 570/630$ nm), which can be attributed to the formation of dye dimers [39,40], as well as a low intensity (due to quenching) green emission. This was used to for the quantification of the drug (i.e., protein) encapsulation (Section 3.1) and time-dependent leaching as well as the release due to capsule degradation in different solutions (Section 3.2). Proteins leached/released from the capsules are subject to enzymatic degradation by cellular proteases. Upon cleavage of DQ-OVA into peptide fragments, the self-quenching of BODIPY is revoked, and its green fluorescence emission increases [30,41,42]. This green fluorescence was used for the analysis of the release profile (Section 3.3).

The efficiency of the DQ-OVA loading cavity was thus estimated by determining the red fluorescence from the CLSM images of the capsule interior, which was integrated along the whole area of the capsule (Fig. 2). To do so, an aqueous suspension of capsules with different architectures and loaded with DQ-OVA were observed with CLSM, and the fluorescence in both, the red and green channels, as well as a transmission image, were collected. To minimize bleaching, the acquisition parameters were tuned to detect fluorescence at very low excitation power. The estimation of the amount of the encapsulated protein was obtained from the red fluorescence images by image analysis using

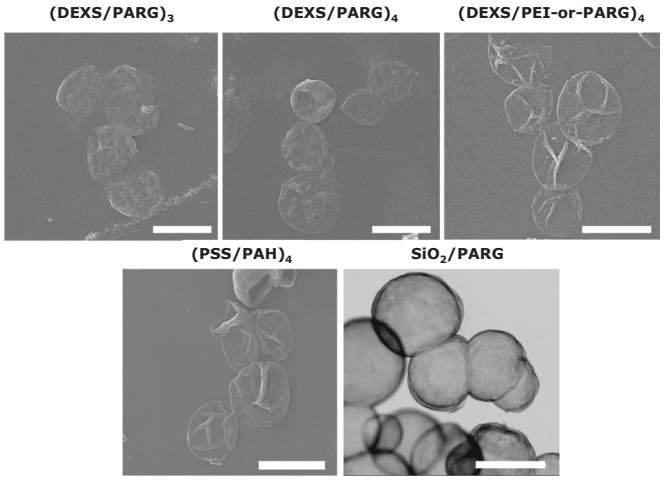

Fig. 1. Capsules characterization. Representative SEM images of $(DEXS/PARG)_3$, $(DEXS/PARG)_4$, $(DEXS/PEI\text{-}or\text{-}PARG)_4$, $(PSS/PAH)_4$, and STEM images of SiO_2/PARG capsules. For SiO_2/PARG capsules the formation of hollow spheres can be seen. The scale bars correspond to 5 μm.

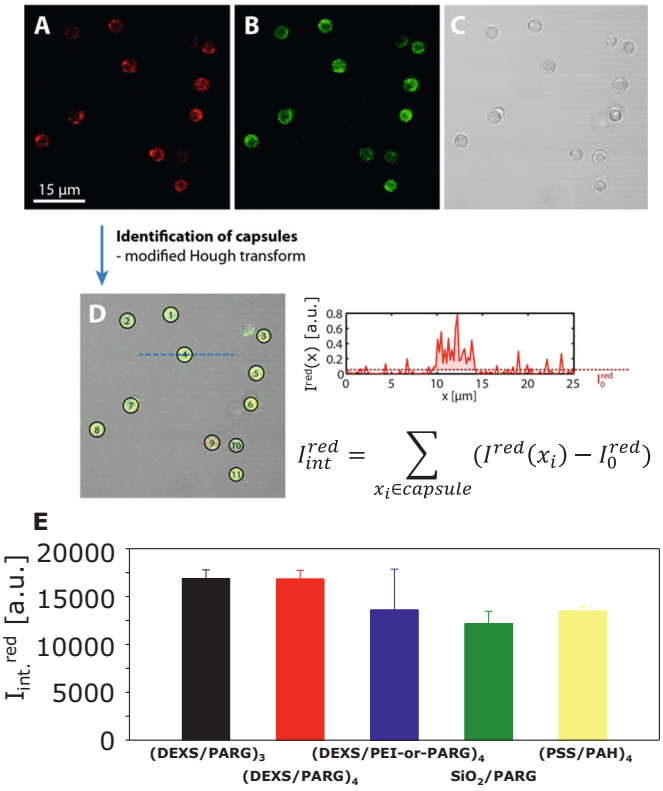

Fig. 2. Capsules characterization. CLSM images of A. Red channel, B. Green channel, C. Transmission channel, D. Identified capsules and example of fluorescence profile $I^{red}(x)$. The fluorescence profile is shown for 4th capsule. The integrated red fluorescence within identified capsule is calculated as shown, by integrating the background-corrected intensity over all pixel positions x_i which are inside the capsule. The methodology is illustrated for SiO_2/PARG capsules. E. Mean value over all analysed cells of the integrated red intensity for each capsule architecture (I_{int}^{red}). Note that the actual green intensity emission (B) is much lower than the red emission (A), and the first has been highlighted for a better visualization. (For interpretation of the references to colour in this figure legend, the reader is referred to the web version of this article.)

Matlab (Mathworks, USA). First, capsules were identified with a modified Hough transform [43,44], and a threshold intensity value for the red fluorescence ($I_{0,}^{red}$) was manually defined to distinguish capsules from the image background. The red intensity was then integrated over the capsule area. The integrated intensity (I_{int}^{red}), which corresponds to the sum of the fluorescence signal within a defined area (capsule), was calculated. About 500 capsules of each composition were analysed. The average value of the integrated intensities of all analysed capsules from each composition was calculated.

Biodegradable capsules based on DEXS and PARG showed the highest fluorescence, irrespective of the number of polyelectrolyte layers, followed by the PEI-containing capsules, and by the non-biodegradable $(PSS/PAH)_4$ capsules. SiO_2/PARG capsules showed the lowest fluorescence, around 42% less than the capsules based on DEXS and PARG. These numbers are indicators for the protein-loading efficiency of each capsule architecture. Since all capsules were prepared from the same $CaCO_3$ cores loaded with DQ-OVA, even when the final size of the polyelectrolyte-based capsules was slightly larger than the one of the SiO_2/PARG, these data suggest that polyelectrolyte-based capsules have a higher encapsulation efficiency. Such observations may be connected with the different nature of the capsule materials (such as higher porosity of SiO_2, involving that more protein cargo might be lost during the washing processes).

3.2. Stability and release studies in cell medium

The stability of the obtained capsules (i.e., retaining of the encapsulated proteins) with different architectures was checked in cell culture medium. It is known that biological fluids are able to dissolve the shell of biodegradable capsules, thus inducing the release of cargo molecules [15]. The different types of capsules loaded with DQ-OVA and dispersed in cell medium were observed under CLSM for different incubation times (Fig. 3A, illustrated for the case of the SiO_2/PARG capsules), and the average value over all analysed capsules from the integrated intensity (I_{int}^{red}) was continuously calculated over the time of incubation (48 h) (Fig. 3B). Additionally, the average diameters of the capsules were plotted versus the time of incubation in the cell medium (Fig. 3C), as upon degradation the capsules are supposed to decrease in size. As observed, both, the red fluorescence and the capsule diameters of the polyelectrolyte-based capsules remained constant with time, whereas the SiO_2/PARG capsules lost a part of their fluorescence signal (around 30%) until ca. 500 min of incubation time. A decrease in the mean size of the SiO_2/PARG capsules was also observed, with similar relative changes. This loss of the fluorescence intensity signal can be also observed in the CLSM images (Fig. 3A). These data indicate that the degradation of SiO_2-based capsules already starts in the cell culture medium, and may be connected with the lower encapsulation efficiency of such capsules (Section 3.1), when compared with their polymeric counterparts.

Previous studies showed that such SiO_2-based capsules degrade in alkaline buffer solutions, with a higher release of cargo when compared with cold water solutions (pH = 6.2), where almost no cargo release was observed [31]. Moreover, different colloidal silica particles are known to dissolve at alkaline pH values [45–47] and also in body fluids [48,49]. There is also degradation in acidic environment, though less than under alkaline conditions.

In order to evaluate the DQ-OVA release efficiency in different media, another biological fluid (the commercial reagent pronase) was

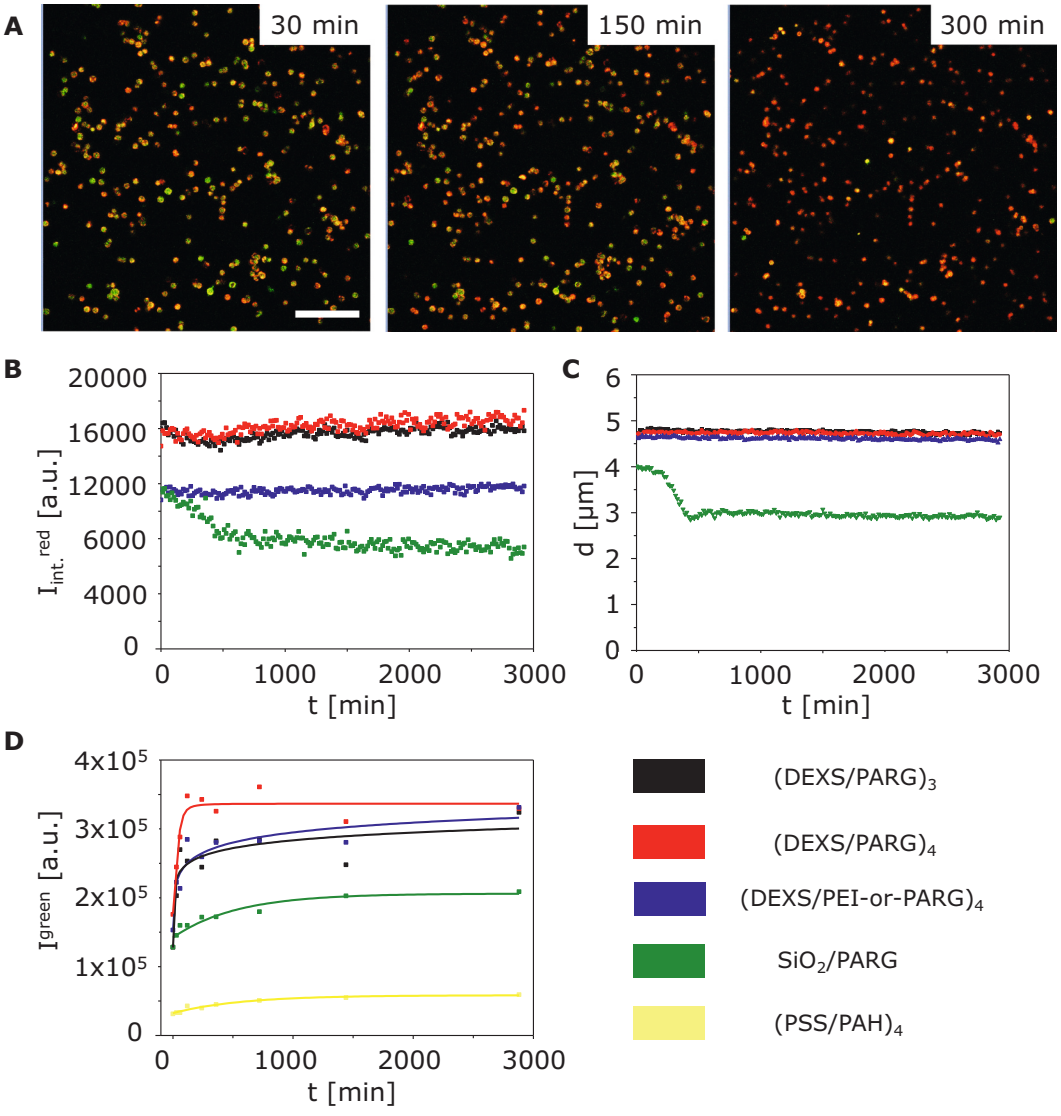

Fig. 3. Stability and release study in cell medium. A. CLSM images of SiO_2/PARG capsules (merged green and red fluorescence signals) incubated in cell culture medium for different time periods. B. Mean red integrated fluorescence intensity from biodegradable DQ-OVA loaded capsules with different architectures with increasing incubation times in cell medium at 37 °C and 5% CO_2. C. Evolution of the diameter d of biodegradable DQ-OVA loaded capsules with different architectures with increasing incubation times t in cell medium at 37 °C and 5% CO_2 as determined from the CLSM images. D. Green fluorescence intensity (recorded at the fluorescence peak $\lambda_{em.} = 512$ nm; $\lambda_{exc} = 483$ nm) of the released DQ-OVA from the same number of DQ-OVA loaded capsules with different architectures after treatment with pronase for increasing times. (For interpretation of the references to colour in this figure legend, the reader is referred to the web version of this article.)

applied. Pronase is a mixture of different proteases whose proteolytic activity extends for a broad range of proteins, including ovalbumin [30,50,51]. In our case pronase plays two different roles: on one hand, it promotes the enzymatic degradation of the biodegradable capsule walls. On the other hand, it also causes the enzymatic cleavage of DQ-OVA, which as previously commented on, gives rise to the appearance of a strong green fluorescence. In order to measure this, the different capsule types were incubated with pronase for 48 h, and the green fluorescence intensity of the released cargo (I^{green}) was measured with a fluorimeter at different time points (Fig. 3D). The degradation of the biodegradable capsule walls and the digestion of the DQ-OVA occurred after 4 h of treatment with pronase at 37 °C. The increase of I^{green} is faster with incubation time for the polyelectrolyte-based capsules, when compared to SiO_2/PARG. In fact, after 48 h of incubation with pronase, I^{green} fluorescence associated with the released DQ-OVA increased about 50% for the SiO_2/PARG capsules, whereas it was almost doubled for the $(DEXS/PARG)_4$ capsules. As expected, the non-degradable $(PSS/PAH)_4$ capsules showed no cargo release and, therefore, the protein cargo molecules had remained in the capsules cavity (i.e., the green fluorescence is almost completely quenched in Fig. 3D).

Comparing both biological fluids (cell culture medium and pronase), it can be noted that pronase strongly affects both, biodegradable polyelectrolyte- and silica-based capsules, inducing their degradation within hours, with a faster cargo release for the polyelectrolyte-based capsules.

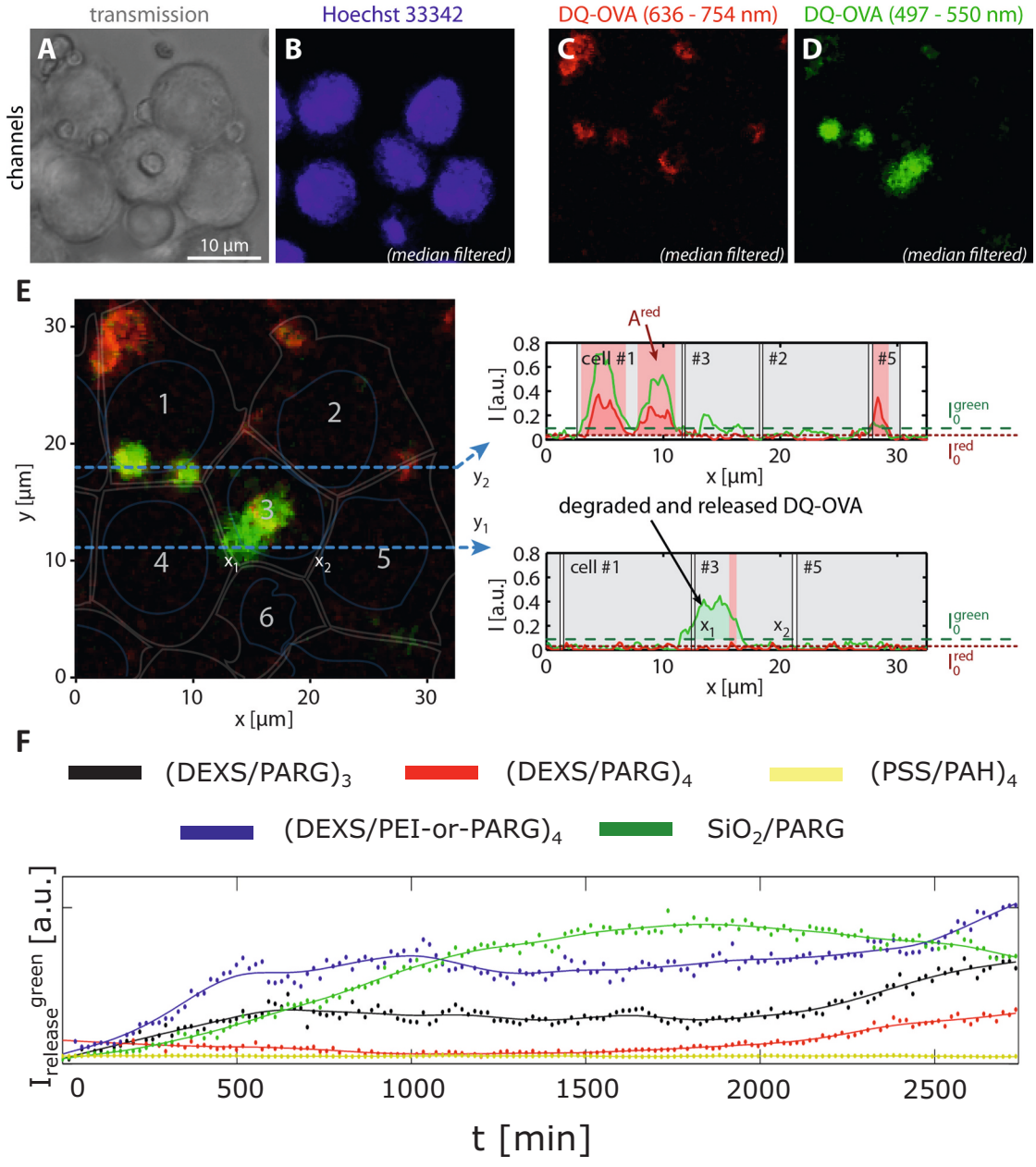

Fig. 4. DQ-OVA release within RAW 264.7 cells. A. transmission picture, B. fluorescence micrograph of nuclei stained with Hoechst 33342 (λ_{exc} = 405 nm, bandpass filter (BP): 420–480 nm, "blue" channel), C. fluorescence micrograph of the "red" signal ("red" channel) coming from BODIPY FL dimers (λ_{exc} = 488 nm, filter: BP 636–754 nm), D. fluorescence micrograph of the "green" signal ("green" channel) coming from BODIPY FL (λ_{exc} = 488 nm, filter: BP 497–550 nm). E. Example of the calculation of fluorescence profiles $I^{green}(x)$ and $I^{red}(x)$ showing the green and red fluorescence originating from the (degraded) DQ-OVA within cells, respectively. F. Quantification of the in-vitro release of DQ-OVA within RAW 264.7 cells from capsules with different architectures with increasing incubation times, provided in terms of $I^{green}_{release}$. Here the mean value of $I^{green}_{release}$ as obtained from different cells is plotted. (For interpretation of the references to colour in this figure legend, the reader is referred to the web version of this article.)

On the contrary, the cell culture medium only influenced the stability of the SiO_2/PARG capsules, and had almost no impact on $(DEXS/PARG)_3$, $(DEXS/PARG)_4$, $(DEXS/PEI\text{-}or\text{-}PARG)_4$ capsules within 48 h.

3.3. In-vitro release of DQ-OVA

The release of encapsulated DQ-OVA after capsule endocytosis inside cells was studied for all the synthesized capsules by collecting both, the red and green fluorescence inside the cells at increasing times. CLSM images were collected and processed with the MatLab and CellProfiler software. At the beginning, cells were identified using the transmission and the additional blue fluorescence channel, in which cell nuclei upon Hoechst 33342 staining were imaged [52]. The red fluorescence was associated with the non-degraded DQ-OVA, and thus with the DQ-OVA remaining in the capsules. Release was defined as the integrated green fluorescence non-colocalized with areas showing red fluorescence, which was also normalized by the red area (which is considered to be approximately proportional to the number of uptaken capsules for each particular cell). The detailed procedure of image processing is described in the Supplementary Data, Figs. S5, S6. Transmission and fluorescence images of RAW 264.7 cells incubated with capsules used for the estimation of the protein release are shown in Fig. 4A-D.

An example of the detailed procedure of the quantification of the DQ-OVA release within one cell in shown in Fig. 4E. The image shows the merged green and red fluorescence signals, which are distributed within the cells. Cell #1 is an example of a cell where no release occurs, since the "green" and "red" fluorescence signals overlap (see the corresponding fluorescence profile shown in the right part of the image). In this case (cell #1), the "green" fluorescence was not taken into account. On the contrary, cell #3 is an example of a cell where the release of DQ-OVA takes place, since the red and green fluorescence signals are no longer colocalized. The fluorescence signal $I^{green}_{release}$ from the released cargo was then calculated as the integral green fluorescence at parts of the cell in which there was no red fluorescence above the background, normalized to the red area of red fluorescence, as described in the Supplementary Data, Fig. S7.

The evolution of $I^{green}_{release}$ inside RAW 264.7 cells that were incubated with all types of DQ-OVA loaded capsules is shown in Figs. 4F and S8. As $I^{green}_{release}$ depends on the green fluorescence signal non-colocalized with the red fluorescence signal that was integrated (summed) within each cell, only the green fluorescence of released and thus degraded DQ-OVA is measured. As $I^{green}_{release}$ is normalized to the area of the red fluorescence signal, which correlates to the number of internalized capsules, it is normalized to the originally delivered amount of DQ-OVA upon endocytosis. As expected, no changes in $I^{green}_{release}$ were observed for the non-biodegradable $(PSS/PAH)_4$ capsules, which is consistent with the absence of cargo release due to non-degradable capsules walls protecting the encapsulated DQ-OVA from degradation. The biodegradable capsules showed different release efficiencies, which can be attributed to the different capsule architectures. A high release efficiency was observed for the $(DEXS/PEI\text{-}or\text{-}PARG)_4$ and SiO_2/PARG capsules. However, both capsules showed different release kinetics. The PEI-containing capsules showed a faster release for times below 1000 min, and from this time until 2500 min higher values of $I^{green}_{release}$ were observed in the SiO_2-based capsules. The slight decrease in the fluorescence intensity observed for SiO_2/PARG capsules at longer incubation times might be associated with the partial exocytosis of the cleaved protein fragments, or to a label dilution upon cell division [53]. Capsules based on the biodegradable DEXS and PARG polymers showed less release abilities. $(DEXS/PARG)_3$ capsules demonstrated a more efficient release of DQ-OVA possibly due to the thinner capsule walls and, therefore, a faster degradation than the $(DEXS/PARG)_4$ capsules. The revealed data suggest that the release of DQ-OVA from SiO_2-based capsules was more efficient within 2500 min, compared with their polyelectrolyte-based counterparts. These results indicate a more efficient in-vitro SiO_2 - capsule degradation, which has been associated in the literature with the low density of silica and the hydrolysis of such shells, and with the presence of CH_3O-PEG-SH on their surface [31]. It is also known that silica can be dissolved in both biological [54] and controlled [55] environments, which is also in good agreement with our observations. The presence of PEI in the polyelectrolyte-based capsules increases the release capabilities, when compared with the other polyelectrolyte-based capsules. This can be associated with the possible induction of proton sponge effect by the cationic PEI that could eventually stimulate release of proteins inside cells; however, one should mention also the toxic side effects of PEI [56].

3.4. In-vitro release of GFP

Based on the obtained data, silica-based capsules demonstrated the most efficient release. Therefore, these carriers were used also to deliver GFP into cells. For this, the SiO_2/PARG capsules were in addition to GFP co-loaded with fluorescent dextran-Alexa Fluor 647 (AF 647), which was used as a reference (Fig. S3). The diameter d of the obtained GFP-loaded capsules was 4.24 ± 0.48 μm, as derived from CLSM images.

Since the fluorescence of GFP is pH-dependent [57], the fluorescence stability of GFP loaded SiO_2/PARG capsules was first determined. The fluorescence of the SiO_2/PARG capsules loaded with GFP and AF 647 was measured and integrated at different pH values. It was observed that the green emission of GFP almost disappeared at acidic pH ($pH < 7$), but this loss of fluorescence was reversible, since the fluorescence was recovered when dispersing the capsules again at slightly basic pH (Fig. S9). Additionally, the suppression of the GFP fluorescence was qualitatively checked using HeLa cells. GFP loaded SiO_2/PARG capsules were incubated with cells for 4 h and the fluorescence images were then immediately collected with CLSM (Fig. S10). Given that polyelectrolyte capsules are usually located after internalization in endo/lysosomal compartments [58], which show an acid pH, capsules showed only red fluorescence (AF 647) inside endo/lysosomes, whereas capsules outside cells emitted merged green and red fluorescence, as the fluorescence of AF 647 does not depend on pH.

In order to evaluate the release kinetics of GFP from SiO_2/PARG capsules, they were incubated with HeLa cells. The quantification of the delivery from SiO_2/PARG capsules loaded with GFP was carried out from the fluorescence images detecting stained cell membranes (orange channel), nuclei (blue channel), GFP (green channel), and dextran-AF 647 (red channel), collected at different time periods (Figs. S11, S12). Note that upon capsule degradation and transient endosome/lysosome opening (as proven in a previous study by a pH indicator [31]), part of the encapsulated GFP is released into the cytosol, whereas the dextran-AF 647 due to its high molecular weight remains inside the capsules. At the beginning, cells were identified using the orange fluorescence channel showing the stained cell membrane and the blue fluorescence channel showing the stained cell nuclei. The red fluorescence of dextran-AF 647 indicates the capsules. Release of GFP from the capsules into the cytosol was defined as the integrated green fluorescence non-colocalized with areas showing red fluorescence, which was also normalized by the red area (which is considered to be approximately proportional to the number of uptaken capsules for each particular cell). The detailed image processing procedure is described in the Supplementary Data.

Cell #4 in Fig. 5E is an example of a cell without GFP release, because the red and green fluorescence overlap. Thus, the fluorescence from GFP within this cell was not taken into account. On the contrary, cell #7 in the same figure is an example of a cell showing release of GFP out of the capsules and the surrounding endosomes/lysosomes into the cytosol, since the green fluorescence (GPF) and the red fluorescence (AF 647) are no longer colocalized. The green signal which is non-colocalized with the red signal is measured, integrated, normalized by the red area, resulting in $I^{green}_{release}$.

A release kinetics of GFP was observed, which is similar to the one of the delivery of DQ-OVA with SiO_2/PARG capsules. The release is relatively slow until ca. 500 min of incubation time, reaching a maximum

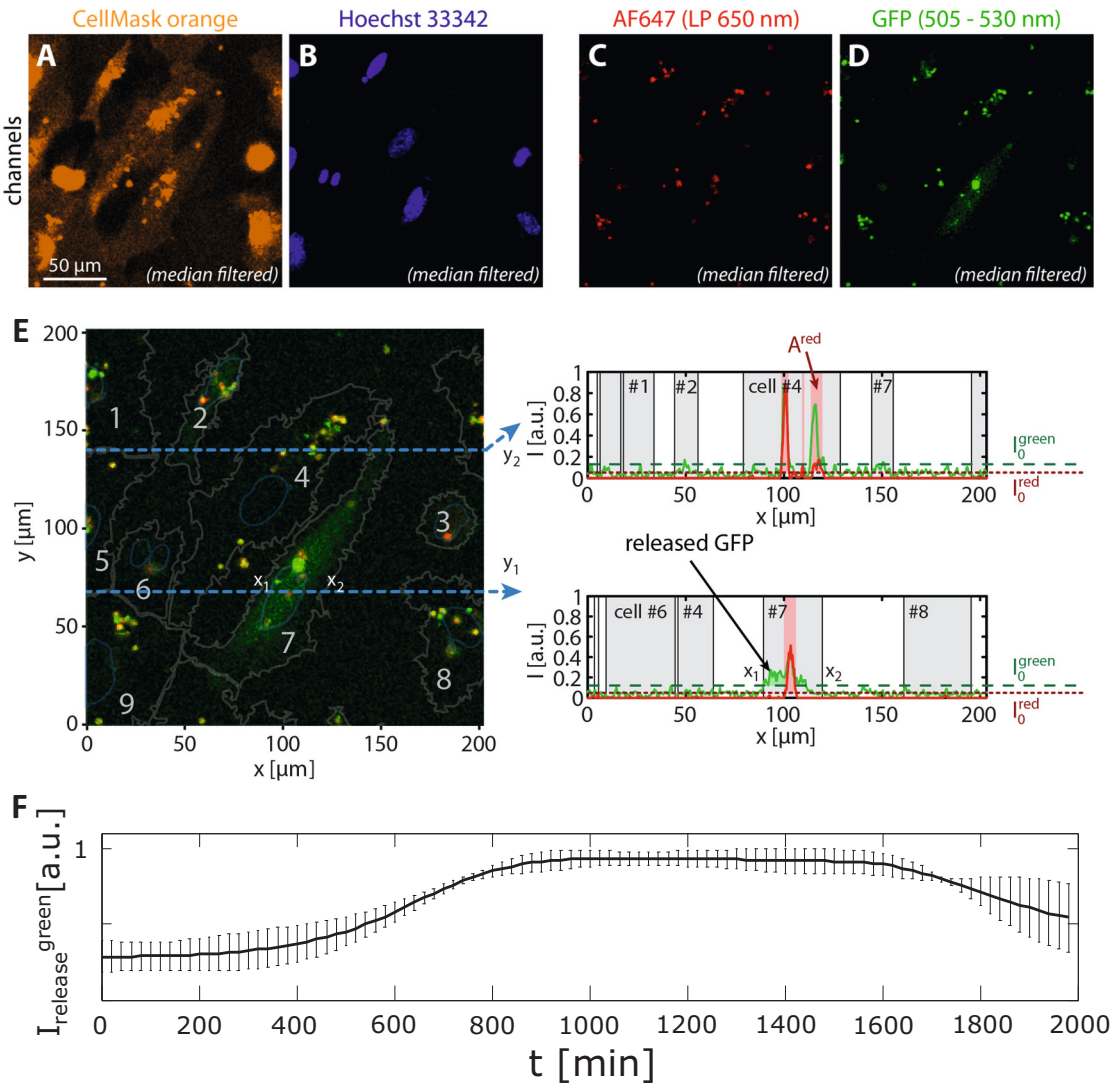

Fig. 5. GFP release within the HeLa cells. A. fluorescence micrograph in the orange channel (λ_{exc} = 543 nm, bandpass filter (BP) for recording the emission: 560–615 nm) showing cell membranes stained with Cell Mask Orange; B. fluorescence micrograph in the blue channel, showing cell nuclei stained with Hoechst 33342 (λ_{exc} = 405 nm, filter: BP 420–480 nm); C. fluorescence micrograph of the "red" signal produced by the reference dye AF 647 (λ_{exc} = 633 nm, long pass (LP) filter: 650 nm); D. fluorescence micrograph of the "green" signal produced by GFP (λ_{exc} = 488 nm, filter: BP 505–550 nm). E. Example of the calculation of fluorescence profiles showing the green and red fluorescence along the indicated lines, originating from the GFP and dextran-AF 647 loaded capsules as endocytosed by HeLa cells. F. Release of GFP within HeLa cells from capsules with different architectures over time. Here the mean value of $I^{green}_{release}$ as obtained from different cells is plotted. (For interpretation of the references to colour in this figure legend, the reader is referred to the web version of this article.)

efficiency at around 900 min of incubation. It is worth mentioning again that after internalization capsules are usually located in endosomal/lysosomal compartments of the cells [58]. These compartments contain enzymes specialized in digesting nutrients, and have acidic environment [42,59,60]. As discussed, the fluorescence of GFP is almost absent at acidic pH values (Figs. S9, S10). Therefore, the green intracellular fluorescence signal coming from proteins would occur due to the following reason: silica-based carriers induce endosomal escape of the delivered cargo [31], leading to translocation into the cytosol, which is close to neutral pH. The location of the released molecules (here GFP) from the SiO_2/PARG capsules is supported by the fact that GFP fluorescence is located now over the volume of the cell and no longer restricted to the location of the capsules inside endosomes/lysosomes, and that the pH change from acid (endosomes/lysosomes) to neutral (cytosol) has been followed with released pH indicators [31,32]. The presence of the capsule carriers and their hydrolyzation also may partly increase the pH inside the endo/lysosomal compartments, which would enhance the green fluorescence of GFP [61]. However, in this case the GFP fluorescence would not spread throughout cells.

4. Conclusions

Protein delivery and release was carried out in-vitro with both, polyelectrolyte- and SiO_2-based micrometric capsules. The encapsulation efficiency and the release kinetics inside and outside cells was determined by processing CLSM images of capsules and cells within 48 h. Polyectrolyte-based capsules demonstrated a better encapsulation efficiency. However, the more efficient release profile within 48 h was observed for SiO_2/PARG capsules, which might however be for the price of increased potential toxicity [31,32]. This can be ascribed to a faster degradation rate of silica-based capsules inside cells, as verified by the performed stability studies. SiO_2/PARG capsules were further applied to deliver GFP into HeLa cells. Release was observed and quantified, resulting in a similar kinetics as for the DQ-OVA loaded capsules. Overall, the developed methodology of the release evaluation inside cells is versatile in terms of used cells and fluorescence compounds, and

allows for analysing and controlling the drug (here protein) release kinetics in order to optimize delivery.

CRediT authorship contribution statement

Funding acquisition, W.J.P., M.Z.V., S.C.R., A.E.; Investigation, M.V. Z., R.H., A.S.T., S.C.R., and A.E.; Resources, W.J.P; Supervision, W.J.P., and A.E.; Writing—original draft, M.V.Z. and A.E.; Writing—review & editing, M.V. Z., R.H., A.S.T., S.C.R., W.J.P., and A.E.

Declaration of competing interest

The authors declare that they have no known competing financial interests or personal relationships that could have appeared to influence the work reported in this paper.

Acknowledgements

This work was supported by the strategic academic leadership program 'Priority 2030' of the Russian Federation (Agreement 75-15-2021-1333 30.09.2021) (MVZ), the Maria de Maeztu Units of Excellence Programme – Grant No. MDM-2017-0720 Ministry of Science, Innovation and Universities, the sixth Research and Technology Transfer Plan of the University of Seville (VI PPIT-US), and the German Research Foundation (DFG, grant PA 794/21-2 to WJP).

Appendix A. Supplementary data

Supplementary data to this article can be found online at https://doi.org/10.1016/j.bioadv.2022.212966.

References

[1] B. Pelaz, C. Alexiou, R.A. Alvarez-Puebla, F. Alves, A.M. Andrews, S. Ashraf, L. P. Balogh, L. Ballerini, A. Bestetti, C. Brendel, S. Bosi, M. Carril, W.C.W. Chan, C. Chen, X. Chen, X. Chen, Z. Cheng, D. Cui, J. Du, C. Dullin, A. Escudero, N. Feliu, M. Gao, M. George, Y. Gogotsi, A. Grünweller, Z. Gu, N.J. Halas, N. Hampp, R. K. Hartmann, M.C. Hersam, P. Hunziker, J. Jian, X. Jiang, P. Jungebluth, P. Kadhiresan, K. Kataoka, A. Khademhosseini, J. Kopeček, N.A. Kotov, H.F. Krug, D.S. Lee, C.-M. Lehr, K.W. Leong, X.-J. Liang, M. Ling Lim, L.M. Liz-Marzán, X. Ma, P. Macchiarini, H. Meng, H. Möhwald, P. Mulvaney, A.E. Nel, S. Nie, P. Nordlander, T. Okano, J. Oliveira, T.H. Park, R.M. Penner, M. Prato, V. Puntes, V.M. Rotello, A. Samarakoon, R.E. Schaak, Y. Shen, S. Sjöqvist, A.G. Skirtach, M. G. Soliman, M.M. Stevens, H.-W. Sung, B.Z. Tang, R. Tietze, B.N. Udugama, J. S. VanEpps, T. Weil, P.S. Weiss, I. Willner, Y. Wu, L. Yang, Z. Yue, Q. Zhang, Q. Zhang, X.-E. Zhang, Y. Zhao, X. Zhou, W.J. Parak, Diverse applications of nanomedicine, ACS Nano 11 (2017) 2313–2381, https://doi.org/10.1021/acsnano.6b06040.

[2] M. Caldorera-Moore, N. Guimard, L. Shi, K. Roy, Designer nanoparticles: incorporating size, shape and triggered release into nanoscale drug carriers, Expert Opin. Drug Deliv. 7 (2010) 479–495, https://doi.org/10.1517/17425240903579971.

[3] S. Stolnik, L. Illum, S.S. Davis, Long circulating microparticulate drug carriers, Adv. Drug Deliv. Rev. 64 (2012) 290–301, https://doi.org/10.1016/j.addr.2012.09.029.

[4] S.R. MacEwan, A. Chilkoti, From composition to cure: a systems engineering approach to anticancer drug carriers, Angew Chem. Int. Ed. Engl. 56 (2017) 6712–6733, https://doi.org/10.1002/anie.201610819.

[5] S.T. Stern, P.P. Adiseshaiah, R.M. Crist, Autophagy and lysosomal dysfunction as emerging mechanisms of nanomaterial toxicity, Part. Fibre Toxicol. 9 (2012).

[6] N. Feliu, J. Hühn, M.V. Zyuzin, S. Ashraf, D. Valdeperez, A. Masood, A.H. Said, A. Escudero, B. Pelaz, E. Gonzalez, M.A.C. Duarte, S. Roy, I. Chakraborty, M.L. Lim, S. Sjöqvist, P. Jungebluth, W.J. Parak, Quantitative uptake of colloidal particles by cell cultures, Sci. Total Environ. 568 (2016) 819–828.

[7] J.B. Delehanty, C.E. Bradburne, K. Boeneman, K. Susumu, D. Farrell, B.C. Mei, J. B. Blanco-Canosa, G. Dawson, P.E. Dawson, H. Mattoussi, I.L. Medintz, Delivering quantum dot-peptide bioconjugates to the cellular cytosol: escaping from the endolysosomal system, Integr. Biol. 2 (2010) 265–277.

[8] R. Lehner, X.Y. Wang, S. Marsch, P. Hunziker, Intelligent nanomaterials for medicine: carrier platforms and targeting strategies in the context of clinical application, nanomedicine-nanotechnologyBiol. Med 9 (2013) 742–757.

[9] Z.-D.H. Wing-Fu Lai, Design and fabrication of hydrogel-based nanoparticulate systems for in vivo drug delivery, J. Control. Release 243 (2016) 269–282, https://doi.org/10.1016/j.jconrel.2016.10.013.

[10] Q.X.Jung Soo Suk Namho Kim, Justin Hanes, Laura M. Ensign, PEGylation as a strategy for improving nanoparticle-based drug and gene delivery, Adv. Drug Deliv. Rev. 99 (2016) 28–51, https://doi.org/10.1016/j.addr.2015.09.012.

[11] I. Koryakina, S.Kuznetsova Daria, A.Zuev Dmitry, A.Milichko Valentin, S. Timin Alexander, V.Zyuzin Mikhail, Optically responsive delivery platforms: from the design considerations to biomedical applications, Nanophotonics 9 (2020) 39, https://doi.org/10.1515/nanoph-2019-0423.

[12] G.P. Zograf, A.S. Timin, A.R. Muslimov, I.I. Shishkin, A. Nominé, J. Ghanbaja, P. Ghosh, Q. Li, M.V. Zyuzin, S.V. Makarov, All-optical nanoscale heating and thermometry with resonant dielectric nanoparticles for controllable drug release in living cells, Laser Photon. Rev. 14 (2020), https://doi.org/10.1002/lpor.201900082.

[13] A.R. Muslimov, A.S. Timin, V.R. Bichaykina, O.O. Peltek, T.E. Karpov, A. Dubavik, A. Nominé, J. Ghanbaja, G.B. Sukhorukov, M.V. Zyuzin, Biomimetic drug delivery platforms based on mesenchymal stem cells impregnated with light-responsive submicron sized carriers, Biomater. Sci. 8 (2020) 1137–1147, https://doi.org/10.1039/C9BM00926D.

[14] A.S. Timin, O.O. Peltek, M.V. Zyuzin, A.R. Muslimov, T.E. Karpov, O. S. Epifanovskaya, A.I. Shakirova, M.V. Zhukov, Y.V. Tarakanchikova, K.V. Lepik, V.S. Sergeev, G.B. Sukhorukov, B.V. Afanasyev, Safe and effective delivery of antitumor drug using mesenchymal stem cells impregnated with submicron carriers, ACS Appl. Mater. Interfaces 11 (2019) 13091–13104, https://doi.org/10.1021/acsami.8b22685.

[15] M.V. Zyuzin, A.S. Timin, G.B. Sukhorukov, Multilayer capsules inside biological systems: state-of-the-art and open challenges, Langmuir 35 (2019) 4747–4762, https://doi.org/10.1021/acs.langmuir.8b04280.

[16] A.S. Timin, A.R. Muslimov, M.V. Zyuzin, O.O. Peltek, T.E. Karpov, I.S. Sergeev, A. I. Dotsenko, A.A. Goncharenko, N.D. Yolshin, A. Sinelnik, B. Krause, T. Baumbach, M.A. Surmeneva, R.V. Chernozem, G.B. Sukhorukov, R.A. Surmenev, Multifunctional scaffolds with improved antimicrobial properties and osteogenicity based on piezoelectric electrospun fibers decorated with bioactive composite microcapsules, ACS Appl. Mater. Interfaces 10 (2018) 34849–34868, https://doi.org/10.1021/acsami.8b09810.

[17] O. Geuli, N. Metoki, T. Zada, M. Reches, N. Eliaz, D. Mandler, Synthesis, coating, and drug-release of hydroxyapatite nanoparticles loaded with antibiotics, J. Mater. Chem. B 5 (2017) 7819–7830, https://doi.org/10.1039/c7tb02105d.

[18] A. Watanabe, M. Takagi, S. Murata, M. Kato, Stability and drug release studies of an antimycotic nanomedicine using HPLC, dynamic light scattering and atomic force microscopy, J. Pharm. Biomed. Anal. 148 (2018) 149–155, https://doi.org/10.1016/j.jpba.2017.09.030.

[19] J.M. Chan, L. Zhang, K.P. Yuet, G. Liao, J.W. Rhee, R. Langer, O.C. Farokhzad, PLGA-lecithin-PEG core-shell nanoparticles for controlled drug delivery, Biomaterials 30 (2009) 1627–1634, https://doi.org/10.1016/j.biomaterials.2008.12.013.

[20] M.V. Zyzin, P. Ramos-Cabrer, S. Carregal-Romero, Encapsulation of enzymes in porous capsules via particle templating, in: Immobil. Enzym. Cells, Springer, 2020, pp. 227–241.

[21] F. Meng, R. Cheng, C. Deng, Z. Zhong, Intracellular drug release nanosystems, Mater. Today 15 (2012) 436–442, https://doi.org/10.1016/s1369-7021(12)70195-5.

[22] N.D. Donahue, H. Acar, S. Wilhelm, Concepts of nanoparticle cellular uptake, intracellular trafficking, and kinetics in nanomedicine, Adv. Drug Deliv. Rev. 143 (2019) 68–96, https://doi.org/10.1016/j.addr.2019.04.008.

[23] M.P. Stewart, R. Langer, K.F. Jensen, Intracellular delivery by membrane disruption: mechanisms, strategies, and concepts, Chem. Rev. 118 (2018) 7409–7531, https://doi.org/10.1021/acs.chemrev.7b00678.

[24] S. Armon, Z. Janet, A. Andrea, S.W. Young, C. Nahyun, J. Emily, M. Shirley, S. Sabine, H. Min-Joon, L.-J. Abigail, J. Siddharth, L. Jungmin, B.P. A., H.D. A., K. J. Woong, H.G. C., K. Kwang-Soo, A.D. G., L. Robert, J.K. F., A vector-free microfluidic platform for intracellular delivery, Proc. Natl. Acad. Sci. 110 (2013) 2082–2087, https://doi.org/10.1073/pnas.1218705110.

[25] Ž. Krpetić, S. Saleemi, I.A. Prior, V. Sée, R. Qureshi, M. Brust, Negotiation of intracellular membrane barriers by TAT-modified gold nanoparticles, ACS Nano 5 (2011) 5195–5201, https://doi.org/10.1021/nn201369k.

[26] A. Wittrup, A. Ai, X. Liu, P. Hamar, R. Trifonova, K. Charisse, M. Manoharan, T. Kirchhausen, J. Lieberman, Visualizing lipid-formulated siRNA release from endosomes and target gene knockdown, Nat. Biotechnol. 33 (2015) 870–876.

[27] C. Leonhardt, G. Schwake, T.R. Stögbauer, S. Rappl, J.T. Kuhr, T.S. Ligon, J. O. Rädler, Single-cell mRNA transfection studies: delivery, kinetics and statistics by numbers, Nanomedicine 10 (2014) 679–688.

[28] V.P. Zhdanov, Kinetics of lipid-nanoparticle-mediated intracellular mRNA delivery and function, Phys. Rev. E 96 (2017) 42406, https://doi.org/10.1103/PhysRevE.96.042406.

[29] Z. Liu, A. Escudero, C. Carrillo-Carrion, I. Chakraborty, D. Zhu, M. Gallego, W. J. Parak, N. Feliu, Biodegradation of bi-labeled polymer-coated rare-earth nanoparticles in adherent cell cultures, Chem. Mater. 32 (2020) 245–254.

[30] P. Rivera-Gil, S. De Koker, B.G. De Geest, W.J. Parak, Intracellular processing of proteins mediated by biodegradable polyelectrolyte capsules, Nano Lett. 9 (2009) 4398–4402.

[31] A. Ott, X. Yu, R. Hartmann, J. Rejman, A. Schütz, M. Ochs, W.J. Parak, S. Carregal Romero, Light-addressable and degradable silica capsules for delivery of molecular cargo to the cytosol of cells, Chem. Mater. 27 (2015) 1929–1942.

[32] M.V. Zyuzin, D. Zhu, W.J. Parak, N. Feliu, A. Escudero, Development of silica-based biodegradable submicrometric carriers and investigating their characteristics as in vitro delivery vehicles, Int. J. Mol. Sci. 21 (2020) 7563.

[33] D.V. Voronin, O.A. Sindeeva, M.A. Kurochkin, O. Mayorova, I.V. Fedosov, O. Semyachkina-Glushkovskaya, D.A. Gorin, V.V. Tuchin, G.B. Sukhorukov, In vitro and in vivo visualization and trapping of fluorescent magnetic microcapsules

in a bloodstream, ACS Appl. Mater. Interfaces 9 (2017) 6885–6893, https://doi.org/10.1021/acsami.6b15811.
[34] M.V. Novoselova, H.M. Loh, D.B. Trushina, A. Ketkar, T.O. Abakumova, T. S. Zatsepin, M. Kakran, A.M. Brzozowska, H.H. Lau, D.A. Gorin, M.N. Antipina, A. I. Brichkina, Biodegradable polymeric multilayer capsules for therapy of lung cancer, ACS Appl. Mater. Interfaces 12 (2020) 5610–5623, https://doi.org/10.1021/acsami.9b21381.
[35] D.S.L. Yana, V. Tarakanchikova, Tatiana Mashel, Albert R. Muslimov, Sergey Pavlov, Kirill V. Lepik, Mikhail V. Zyuzin, Gleb B. Sukhorukov, Alexander S. Timin, Boosting transfection efficiency: a systematic study using layer-by-layer based gene delivery platform, Mater. Sci. Eng. C. 126 (2021), https://doi.org/10.1016/j.msec.2021.112161.
[36] E.N. Gerasimova, V.V. Yaroshenko, P.M. Talianov, O.O. Peltek, M.A. Baranov, P. V. Kapitanova, D.A. Zuev, A.S. Timin, M.V. Zyuzin, Real-time temperature monitoring of photoinduced cargo release inside living cells using hybrid capsules decorated with gold nanoparticles and fluorescent nanodiamonds, ACS Appl. Mater. Interfaces 13 (2021) 36737–36746, https://doi.org/10.1021/acsami.1c05252.
[37] M.V. Zyuzin, P. Díez, M. Goldsmith, S. Carregal-Romero, C. Teodosio, J. Rejman, N. Feliu, A. Escudero, M.J. Almendral, U. Linne, D. Peer, M. Fuentes, W.J. Parak, Comprehensive and systematic analysis of the immunocompatibility of polyelectrolyte capsules, Bioconjug. Chem. 28 (2017) 556–564.
[38] S. De Koker, L.J. De Cock, P. Rivera-Gil, W.J. Parak, R.A. Velty, C. Vervaet, J. P. Remon, J. Grooten, B.G. De Geest, Polymeric multilayer capsules delivering biotherapeutics, Adv. Drug Deliv. Rev. 63 (2011) 748–761.
[39] F. Bergstroem, I. Mikhalyov, P. Haeggloef, R. Wortmann, T. Ny, L.B.A. Johansson, Dimers of dipyrrometheneboron difluoride (BODIPY) with light spectroscopic applications in chemistry and biology, J. Am. Chem. Soc. 124 (2002) 196–204.
[40] I. Mikhalyov, N. Gretskaya, F. Bergstroem, L.B.A. Johansson, Electronic ground and excited state properties of dipyrrometheneboron difluoride (BODIPY): dimers with application to biosciences, Phys. Chem. Chem. Phys. 4 (2002) 5663–5670.
[41] M.K. Mansour, E. Latz, S.M. Levitz, Cryptococcus neoformans glycoantigens are captured by multiple lectin receptors and presented by dendritic cells, J. Immunol. 176 (2006) 3053–3061.
[42] M. Chanana, P. Rivera Gil, M.A. Correa-Duarte, W.J. Parak, L.M. Liz-Marzán, Physicochemical properties of protein-coated gold nanoparticles in biological fluids and cells before and after proteolytic digestion, Angew. Chemie, Int. Ed. 52 (2013) 4179–4183, https://doi.org/10.1002/anie.201208019.
[43] R. Hartmann, M. Weidenbach, M. Neubauer, A. Fery, W.J. Parak, Stiffness-dependent in vitro uptake and lysosomal acidification of colloidal particles, Angew. Chemie Int. Ed. 54 (2015) 1365–1368.
[44] R.C. Gonzalez, R.E. Woods, Digital Image Processing, Pearson Education, Upper Saddle River, NJ, 2008.
[45] S. Zhang, Z. Chu, C. Yin, C. Zhang, G. Lin, Q. Li, Controllable drug release and simultaneously carrier decomposition of SiO2-drug composite nanoparticles, J. Am. Chem. Soc. 135 (2013) 5709–5716, https://doi.org/10.1021/ja3123015.
[46] P.M. Dove, N. Han, A.F. Wallace, J.J. De Yoreo, Kinetics of amorphous silica dissolution and the paradox of the silica polymorphs, Proc. Natl. Acad. Sci. U. S. A. 105 (2008) 9903–9908.
[47] H. Yamada, C. Urata, Y. Aoyama, S. Osada, Y. Yamauchi, K. Kuroda, Preparation of colloidal mesoporous silica nanoparticles with different diameters and their unique degradation behavior in static aqueous systems, Chem. Mater. 24 (2012) 1462–1471, https://doi.org/10.1021/cm3001688.
[48] G.T. Chen Zhaogang, Xiaodan Su, Ying Liu, Guangming Lu, Unique biological degradation behavior of Stöber mesoporous silica nanoparticles from their interiors to their exteriors, J. Biomed. Nanotechnol. 11 (2015) 722–729, https://doi.org/10.1166/jbn.2015.2072.
[49] S.C. Shen, W.K. Ng, Z. Shi, L. Chia, K.G. Neoh, R.B. Tan, Mesoporous silica nanoparticle-functionalized poly(methyl methacrylate)-based bone cement for effective antibiotics delivery, J. Mater. Sci. Mater. Med. 22 (2011) 2283–2292, https://doi.org/10.1007/s10856-011-4397-1.
[50] J.F. Foley, B.T. Aftonomos, Chapter 1 - Pronase, in: P.F. Kruse, M.K. Patterson (Eds.), Tissue Cult., 1973, pp. 185–188, https://doi.org/10.1016/B978-0-12-427150-0.50051-6.
[51] Roche, Pronase From Streptomyces Griseus, (n.d.).
[52] J. Bucevičius, G. Lukinavičius, R. Gerasimaitė, The use of hoechst dyes for DNA staining and beyond, Chemosensors. 6 (2018) 18, https://doi.org/10.3390/chemosensors6020018.
[53] D. Bartczak, S. Nitti, T.M. Millar, A.G. Kanaras, Exocytosis of peptide functionalized gold nanoparticles in endothelial cells, Nanoscale 4 (2012) 4470–4472, https://doi.org/10.1039/C2NR31064C.
[54] V. Cauda, A. Schlossbauer, T. Bein, Bio-degradation study of colloidal mesoporous silica nanoparticles: effect of surface functionalization with organo-silanes and poly(ethylene glycol), Microporous Mesoporous Mater. 132 (2010) 60–71.
[55] Y.J. Wong, L. Zhu, W.S. Teo, Y.W. Tan, Y. Yang, C. Wang, H. Chen, Revisiting the Stöber method: inhomogeneity in silica shells, J. Am. Chem. Soc. 133 (2011) 11422–11425, https://doi.org/10.1021/ja203316q.
[56] A. Akinc, M. Thomas, A.M. Klibanov, R. Langer, Exploring polyethylenimine-mediated DNA transfection and the proton sponge hypothesis, J. Gene Med. 7 (2005) 657–663.
[57] W.W. Ward, Properties of the coelenterate green-fluorescent proteins, in: M.A. M. Deluca, D. William (Eds.), Biolumin. Chemilumin, Academic Press, 1981, pp. 235–242, https://doi.org/10.1016/B978-0-12-208820-9.50035-5.
[58] L. Kastl, D. Sasse, V. Wulf, R. Hartmann, J. Mircheski, C. Ranke, S. Carregal-Romero, J.A. Martínez-López, R. Fernández-Chacón, W.J. Parak, H.-P. Elsaesser, P. Rivera Gil, Multiple internalization pathways of polyelectrolyte multilayer capsules into mammalian cells, ACS Nano 7 (2013) 6605–6618, https://doi.org/10.1021/nn306032k.
[59] J.P. Luzio, P.R. Pryor, N.A. Bright, Lysosomes: fusion and function, Nat. Rev. Mol. Cell Biol. 8 (2007) 622–632.
[60] M. Nazarenus, Q. Zhang, M.G. Soliman, P. del Pino, B. Pelaz, J. Rejman, B. Rothen-Ruthishauser, M.J.D. Clift, R. Zellner, G.U. Nienhaus, J.B. Delehanty, I.L. Medintz, W.J. Parak, S. Carregal-Romero, In vitro Interaction of Colloidal Nanoparticles with Mammalian Cells: What Have We Learned Thus Far? Beilstein J. Nanotechnol. 5 (2014) 1477–1490.
[61] D. Bandyopadhyay, A. Cyphersmith, J.A. Zapata, Y.J. Kim, C.K. Payne, Lysosome transport as a function of lysosome diameter, PLoS One. 9 (2014), e86847, https://doi.org/10.1371/journal.pone.0086847.